# Supporting Information

## Biodegradable and Flexible Polymer Based Memristor Possessing Optimized Synaptic Plasticity for Eco-Friendly Wearable Neural Networks with High Energy Efficiency

*Sungjun. Oh, Hyungjin. Kim, Seong Eun. Kim, Min-Hwi. Kim, Hea-Lim. Park, and Sin-Hyung. Lee*,*

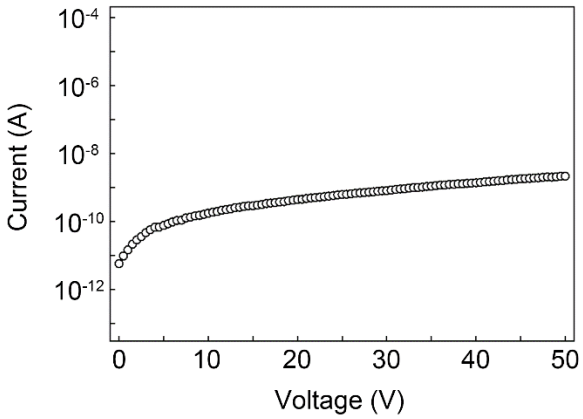


**Figure S1.** Current–voltage characteristics of the planar-type organic memristor consisting of poly (vinyl alcohol) with the molecular weight of 130000 $gmol^{-1}$. Resistive switching characteristics were not observed in the device.

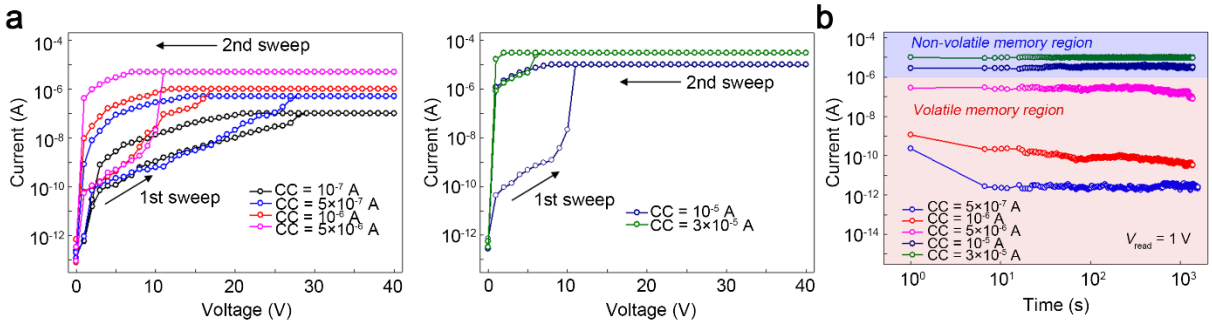


**Figure S2.** (a) Current–voltage curves of the lateral-type memristor with $M_w$ = 10000 gmol$^{-1}$ according to the successive voltage sweeps with different compliance currents (CCs): CC = $10^{-7}$ A, $5\times10^{-7}$ A, $10^{-6}$ A, $5\times10^{-6}$ A, $10^{-5}$ A, and $3\times10^{-5}$ A. (b) Memory retention properties of the device after the resistive switching processes with the different CC values.

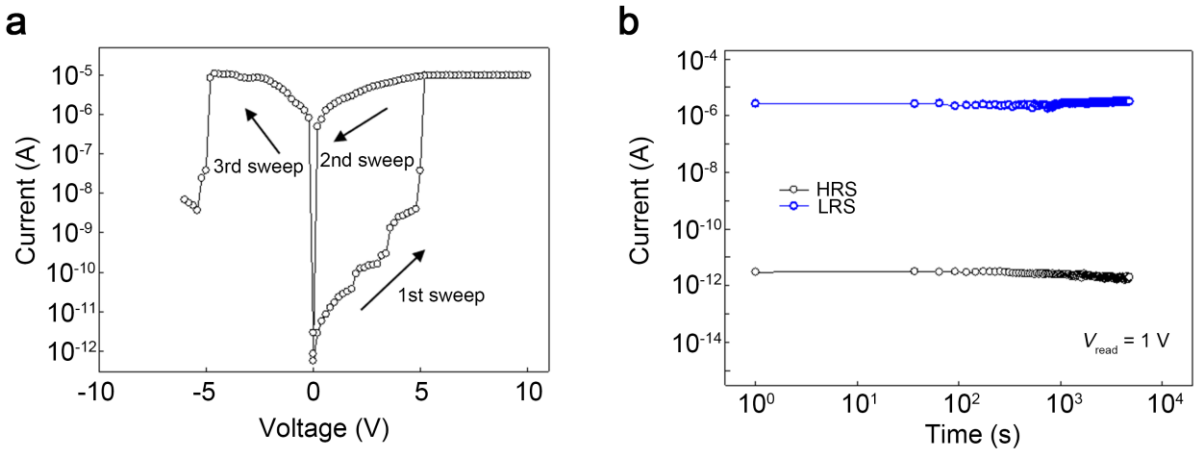


**Figure S3.** Reversible resistive switching characteristics of the poly (vinyl alcohol)-based memristor with a planar structure. (a) Current–voltage curves of the device. (b) Memory retention characteristics of the device at each memory state: high resistance state (HRS) and low resistance state (LRS).

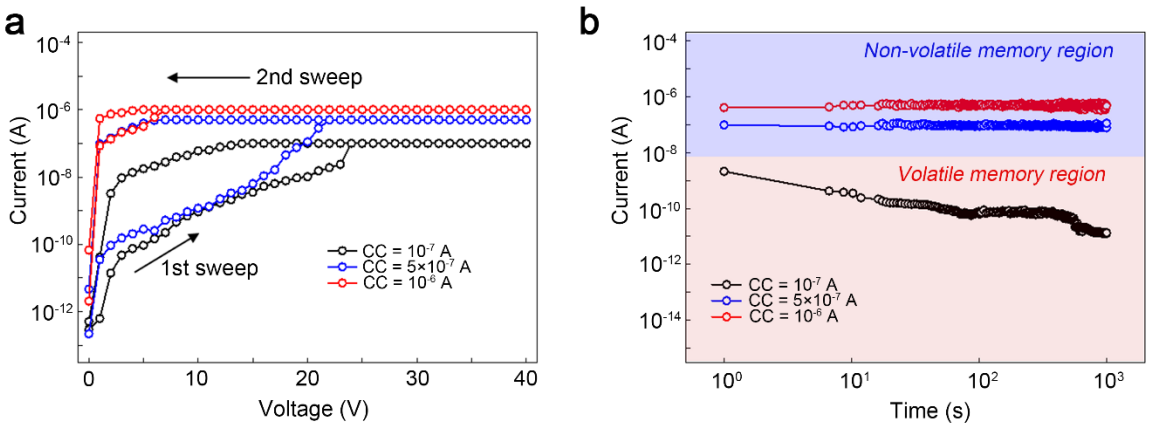


**Figure S4.** (a) Current–voltage curves of the lateral-type memristor with $M_w$ = 23000 gmol$^{-1}$ according to the successive voltage sweeps with different compliance currents (CCs): CC = $10^{-7}$ A, $5\times10^{-7}$ A, and $10^{-6}$ A. (b) Memory retention properties of the device after the resistive switching processes with the different CC values.

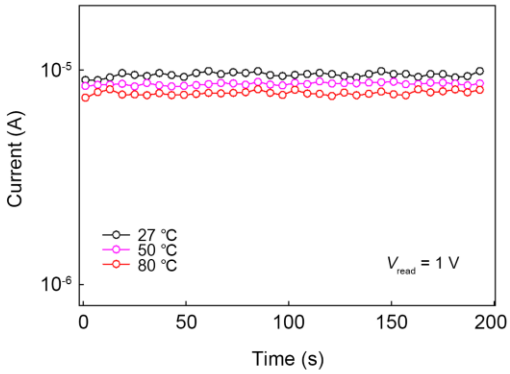


**Figure S5.** The retention test of the poly (vinyl alcohol)-based memristor with a planar structure at the LRS under temperature for a range of 27 ~ 80 ℃. The resistive switching process of the device was performed at the CC = $3\times10^{-5}$ A.

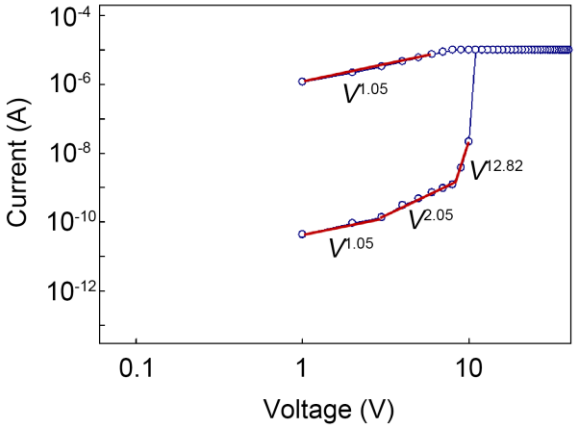


**Figure S6.** Log−log current−voltage curves with local linear fitting of the poly (vinyl alcohol)-based memristor with a planar structure. The polymer $M_w$ for the device was 10000 $gmol^{-1}$.

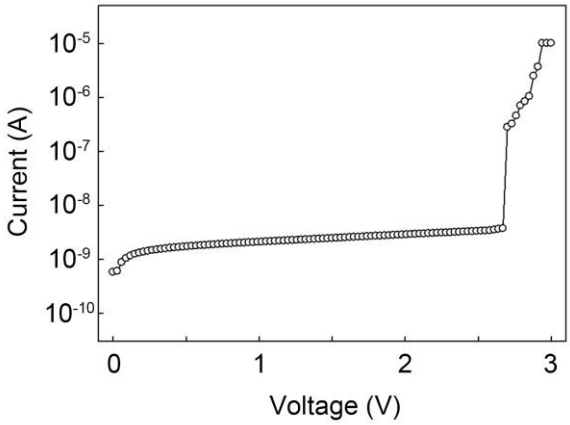


**Figure S7.** An electroforming process to trigger the metallic conductive filament in the poly (vinyl alcohol)-based memristor with a vertical structure.

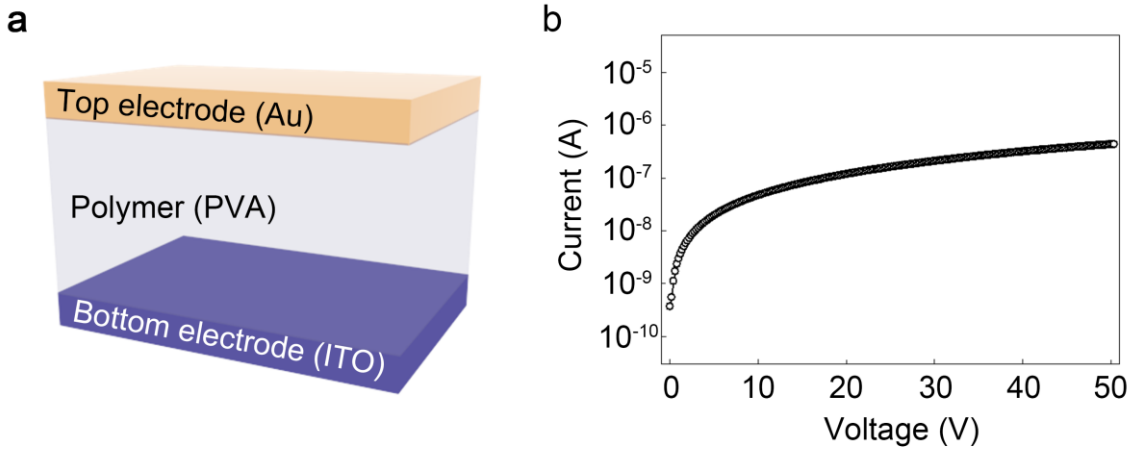


**Figure S8.** The gold/poly (vinyl alcohol) (PVA)/indium tin oxide structured device for confirming the effect of the hydroxyl groups in the polymer on the resistive switching behavior of the PVA based memristor. (a) A schematic showing the device structure for analyzing the hydroxyl group effect. (b) A current−voltage curve for the device. Resistive switching characteristics were not observed in the device, which indicates that the hydroxyl group effect is not related with the memory behaviors of the developed PVA based memristor.

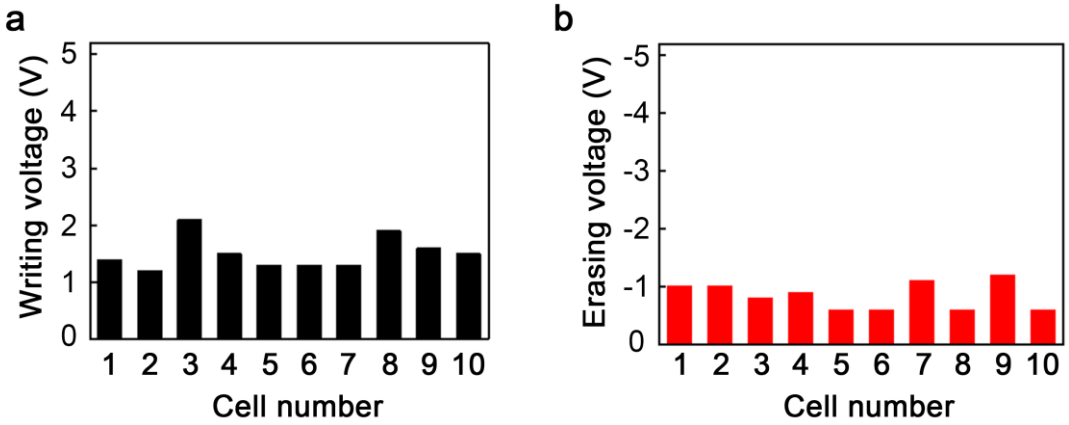


**Figure S9.** Dispersions of (a) the writing and (b) erasing voltages investigated in 10 different cells of the vertical-type poly (vinyl alcohol) based memristor. The cell number refers to an individual cell.

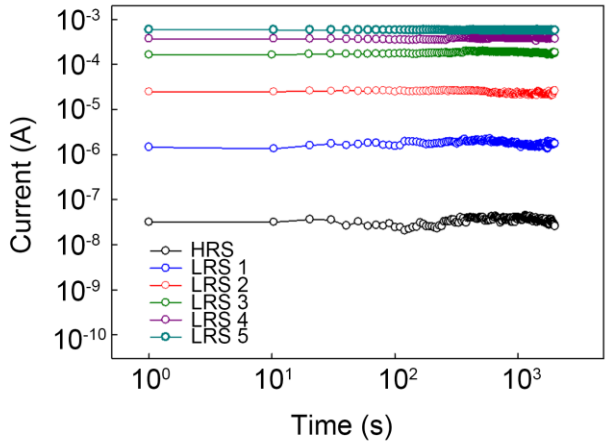


**Figure S10.** Memory retention characteristics of the poly (vinyl alcohol) based memristor at the different conductance states. Each memory conductance of the device was obtained by the compliance current conditions in Fig. 2g.

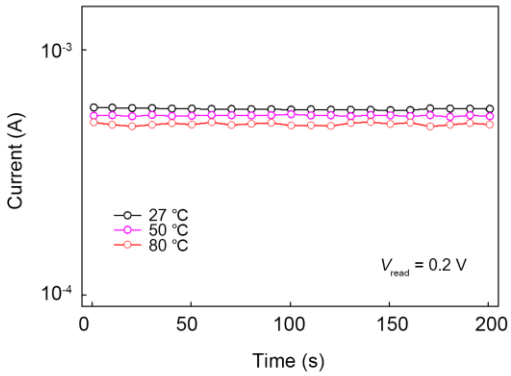


**Figure S11.** The retention test of the poly (vinyl alcohol)-based memristor with a vertical structure at the LRS 5 under temperature for a range of 27 ~ 80 ℃. The temperature coefficient of resistance was calculated as 0.0037 $K^{-1}$, which is similar to that of Ag (~0.0038 $K^{-1}$).

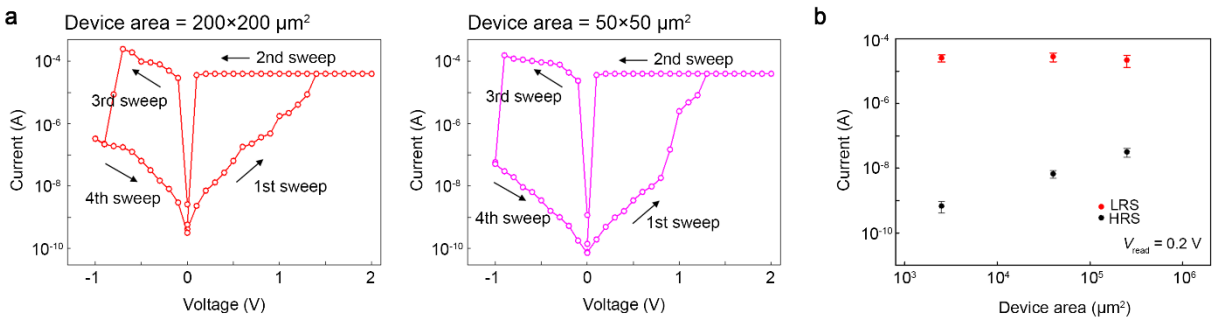


**Figure S12.** Resistive switching behaviors of the vertical-type poly (vinyl alcohol) based memristors with different cell areas (200×200 μm$^2$ and 50×50 μm$^2$). (a) Current–voltage characteristics of the devices (b) Conductance values of the device as a function of the cell area.

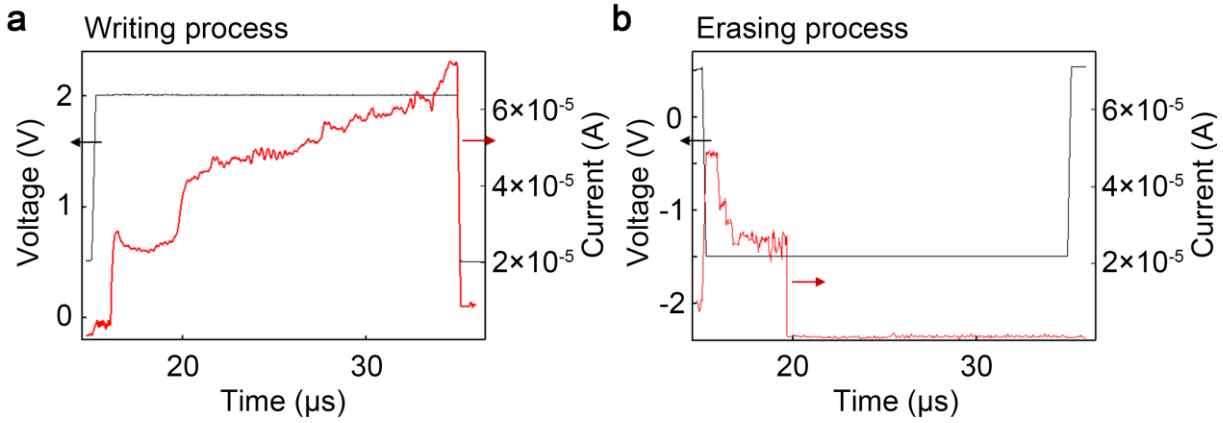


**Figure S13.** Pulse operation of the poly (vinyl alcohol) based memristor with a vertical structure. (a) A voltage pulse with the amplitude of 2.0 V was used for writing and (b) the pulse with the amplitude of -1.5 V was used for erasing. The switching times for writing and erasing were about 5.3 μs and 5.0 μs respectively.

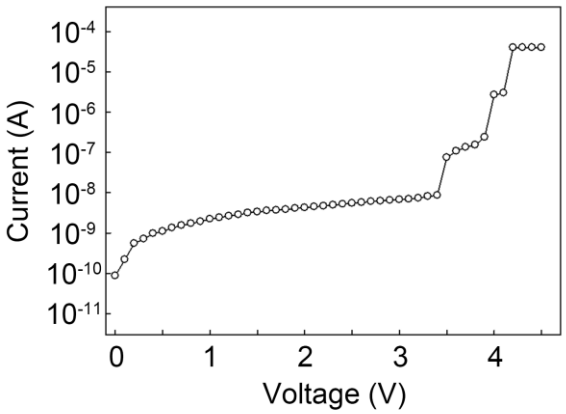


**Figure S14.** An electroforming process to trigger the metallic conductive filament in the poly (vinyl alcohol)-based flexible memristor.

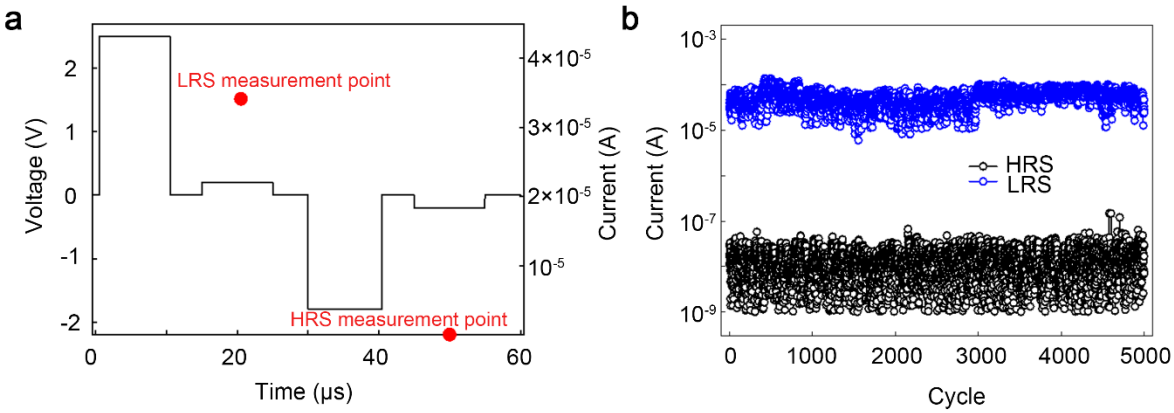


**Figure S15.** (a) The voltage pulse conditions for cycle test of the flexible transient memritor. The red points measured at 0.2 V present the data points in each cycle. (b) The endurance characteristics of the device under the pulse stresses.

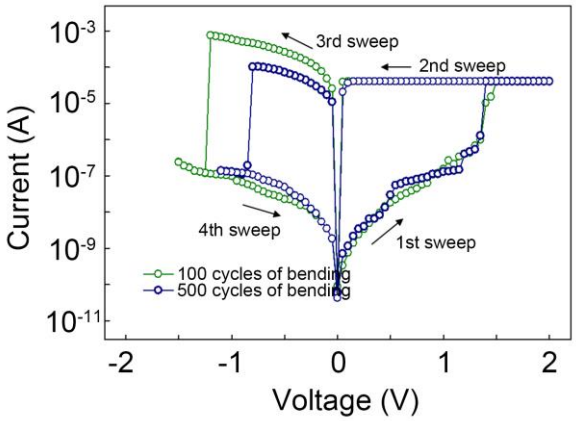


**Figure S16.** The reversible resistive switching characteristics of the poly (vinyl alcohol) based flexible memristor after the mechanical bending stresses.

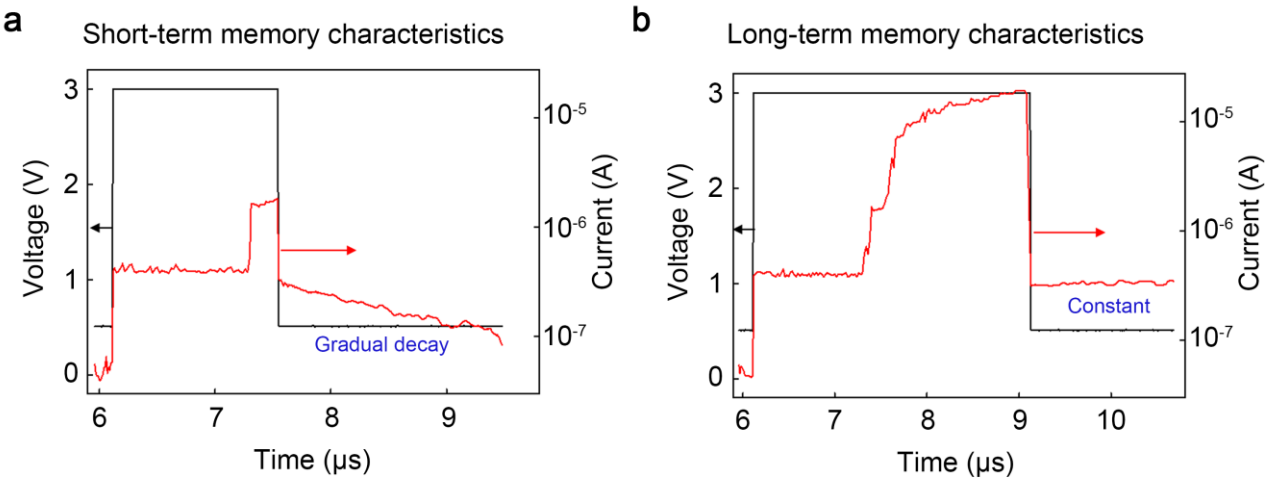


**Figure S17.** Short- and long-term memory characteristics in the poly (vinyl alcohol) based flexible memristor. (a) A transient response of the memristor under the short voltage pulse (1.5 μs width). The device was operated as a volatile memory. (b) The response of the device at the long voltage pulse (3.0 μs width). The device showed the non-volatile memory characteristics.

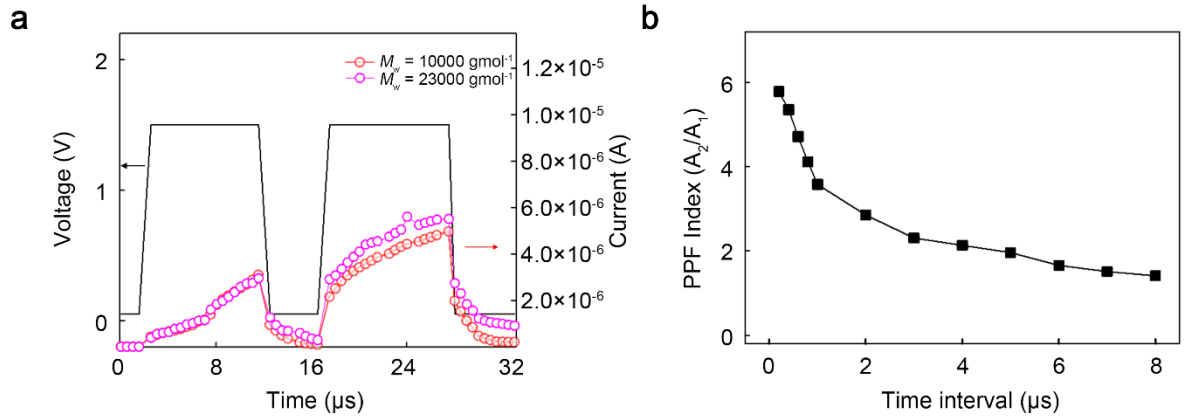


**Figure S18.** (a) Excitatory post-synaptic currents of the vertical type memristors with $M_w$ = 10000 and 23000 gmol$^{-1}$, under electric stimuli. (b) Paired-pulse facilitation (PPF) index as a function of a time interval value between two successive voltage pulses (1.5 V, 10 μs), in the vertical type memristor with $M_w$ = 23000 gmol$^{-1}$.

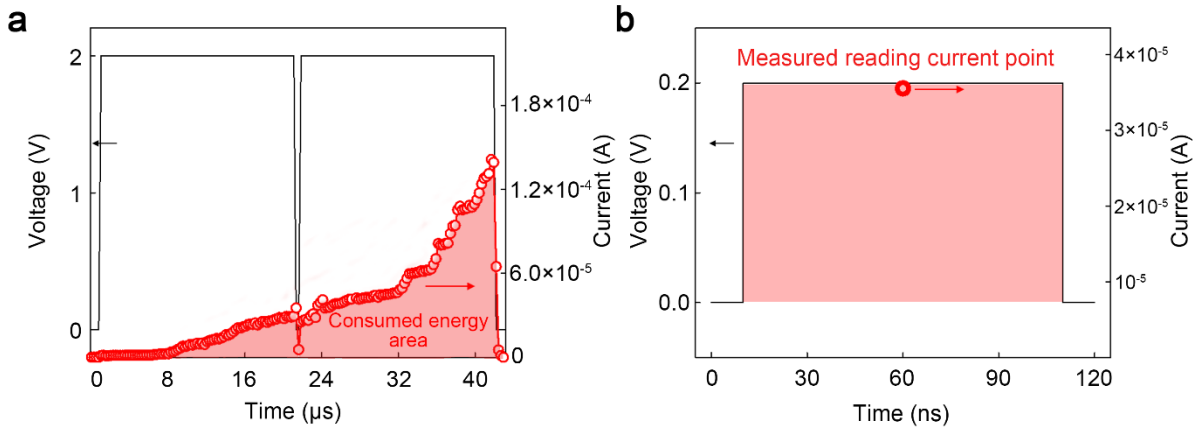


**Figure S19.** Analysis for the consumed energy in the memristor arrays. (a) For training the cell, the consumed energy was calculated by the multiplication of the writing pulse amplitude and the consumed energy area. The consumed energy area was estimated by the writing pulse width and current values. (b) For the computation, the consumed energy in the bit line was calculated by the multiplication of the reading current, the reading pulse width and amplitude.

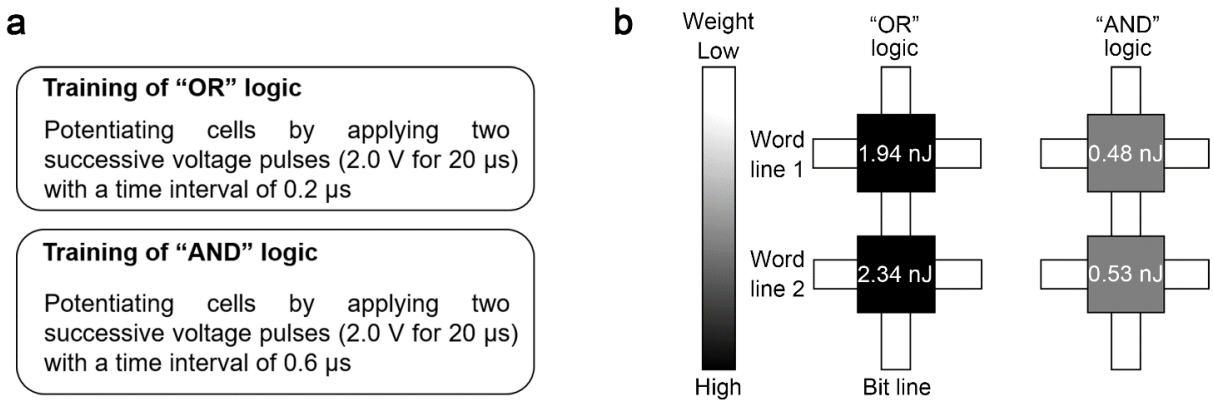


**Figure S20.** Training of "OR" and "AND" logics to the developed neural networks. (a) A flow chart for training logics to the developed neural network. (b) The ideal weight distribution of the synapse cells for the operation of "OR" and "AND" logics, and the consumed energy for training each logic. For training "OR" and "AND" logics, about 4.28 and 1.01 nJ were consumed, respectively.

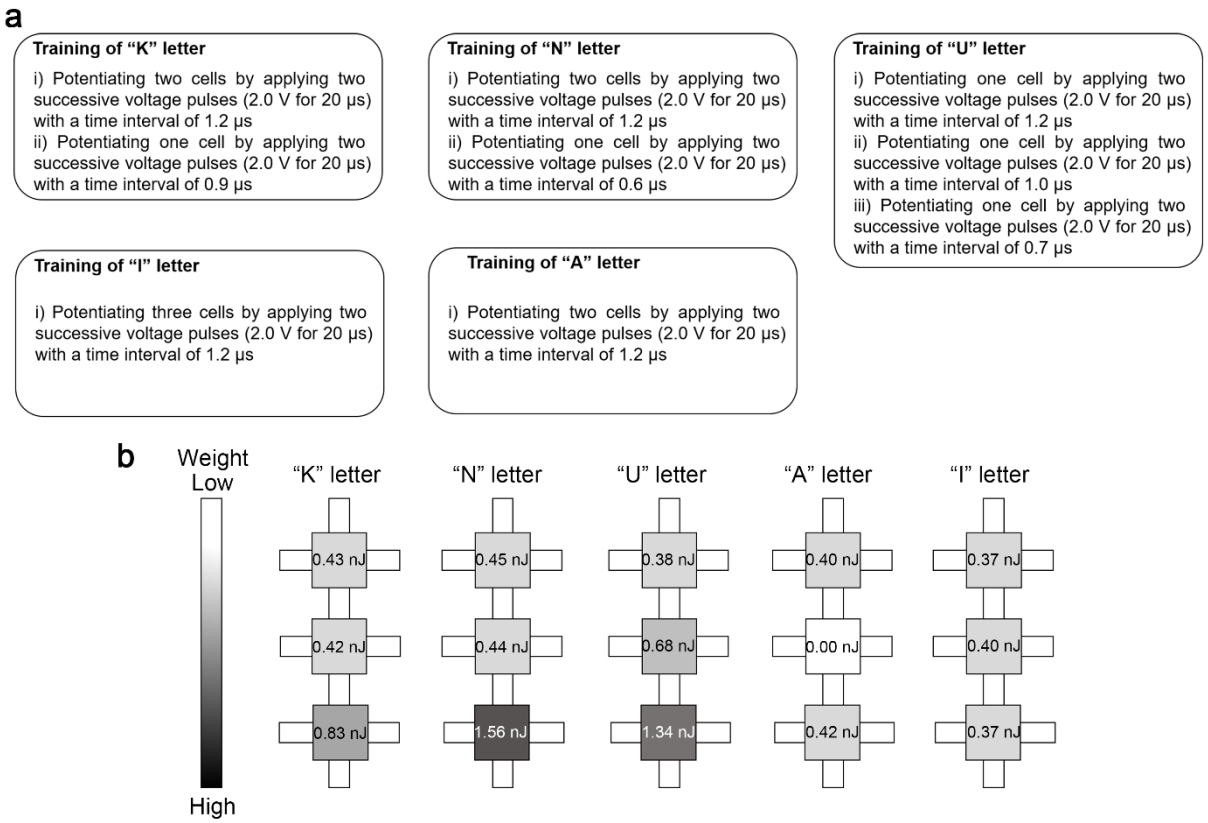


**Figure S21.** Training of "K", "N", "U", "A", and "I" letters to the developed neural networks. (a) A flow chart for training logics to the developed neural network. (b) The ideal weight distribution of the synapse cells for the operation of the letters, and the consumed energy for training each letter. For training "K", "N", "U", "A" and "I" letters, about 1.68, 2.45, 2.40, 0.82, and 1.14 nJ were consumed, respectively.

| Device structure | Mechanism | Write/Erase voltage | Synaptic emulation | Fabricated neural network | Ref. |
|---|---|---|---|---|---|
| Au/PVA/ITO | Dipole alignment | 0.5 V / -0.5 V | STP, PPF, SRDP | - | [38] |
| Al/ZnO-doped PVA/PEDOT:PSS/Al | Ion migration | 4.0 V / -4.0 V | LTP | - | [35] |
| Ag/Ag-doped PVA/Pt | Filamentary conduction | 1.0 V / -0.6 V | LTP | - | [39] |
| Au/PVA/Graphene oxide-embedded PVA/PVA/Au | Ion migration | 3.8 V / -3.2 V | LTP | - | [36] |
| Ag/Iron oxide-embedded PVA/FTO | Ion migration | 2.0 V / -1.5 V | LTP | - | [37] |
| Ag/PVA/ITO | Electrochemcial metallization | 1.5 V / -1.5 V | STP/LTP, EPSC, PPF, SRDP, SNDP, multilevel memory states | AND / OR / ASCII letter logics based on spike-depedent operation | This work |

**Table S1.** Comparison of performances of memristors comprising poly (vinyl alcohol) (PVA).

| Device structure | Mechanism | Write/Erase voltage | Synaptic emulation | Dissolving time | Ref. |
|---|---|---|---|---|---|
| Mg/albumen/W | Ion migration | 1.3 V / -1.0 V | LTP | 72 h | [21] |
| Ag/MgO/Ag | Electrochemcial metallization | 1.0 V / -1.0 V | LTP | 8 min | [24] |
| Mg/Ag-doped chitosan/ITO | Electrochemcial metallization | 2.0 V / -2.0 V | LTP | 90 min | [20] |
| Mg/ZnO/W | Electrochemcial metallization | -2.0 V / 2.0 V | LTP | 15 min | [25] |
| Au/Mg/fibroin /Mg | Electrochemcial metallization | 2.0 V / -1.0 V | LTP | 2 h | [22] |
| Mg/MgO/Mg | Electrochemcial metallization | 4.0 V / -4.0 V | LTP | 30 min | [23] |
| W/silk fibroin/Mg | Electrochemcial metallization | 3.0 V / -3.0 V | LTP | 24 h | [26] |
| Ag/keratin/FTO | Electrochemcial metallization | 1.5 V / -1.2 V | LTP | 30 min | [27] |
| Ag/α-lactose/ITO | Electrochemcial metallization | 1.5 V / -1.5 V | Multilevel memory states | 3 s | [29] |
| Ag/pectin/ITO | Electrochemcial metallization | 1.5 V / -1.5 V | LTP | 10 min | [27] |
| Cu/honey/$Cu_xO$ | Electrochemcial metallization | 1.5 V / -1.5 V | LTP, SRDP | 3 min | [30] |
| Ag/PVA/ITO | Electrochemcial metallization | 1.5 V / -1.5 V | STP/LTP, EPSC, PPF, SRDP, SNDP, multilevel memory states | 30 s | This work |

**Table S2.** Comparison of performances of transient memristors.